High lineage survivorship across the end-Devonian Mass Extinction suggested by a remarkable new Late Devonian actinopterygian

Sam Giles[a,b,*], Kara Feilich[c], Rachel Warnock[d], Stephanie E. Pierce[e], Matt Friedman[b,f]

[a]School of Geography Earth and Environmental Sciences, University of Birmingham, Birmingham B15 2TT, UK; [b]Department of Earth Sciences, Natural History Museum, Cromwell Road, London SW7 5BD, UK; [c]Department of Earth and Environmental Sciences, University of Michigan, 1105 N University Ave, Ann Arbor, MI 48109, USA.; [d]GeoZentrum Nordbayern, Friedrich-Alexander-Universität Erlangen-Nürnberg, Loewenichstraße 28, 91054 Erlangen Germany; [e]Museum of Comparative Zoology and Department of Organismic and Evolutionary Biology, Harvard University, 26 Oxford Street, Cambridge, MA 02138, USA; [f]Museum of Paleontology and Department of Earth and Environmental Sciences, University of Michigan, 1105 N University Ave, Ann Arbor, MI 48109, USA.

*Corresponding author: Sam Giles, s.giles.1@bham.ac.uk.

Keywords: mass extinction; ray-finned fishes; diversification; CT scanning; Devonian; Carboniferous.

Abstract

Actinopterygian (ray-finned) fishes represent the principal vertebrate group in aquatic settings. This dominance is often attributed to their apparent success in the aftermath of the end-Devonian extinction. Increases in taxonomic and morphological diversity in the early Carboniferous, coupled with phylogenetic hypotheses implying the survival of few Devonian lineages, contribute to a model of explosive post-extinction radiation. However, most actinopterygian fossils from within a ca. 20 million year (Myr) window surrounding the end-Devonian extinction remain poorly known, contributing to uncertainty about these patterns. Here we present detailed anatomical data for an exceptionally preserved but diminutive ray-finned fish from within this gap, ~7 Myr prior to the Devonian-Carboniferous boundary. Representing a new genus and species, it bears a series of derived anatomical features otherwise known only from Carboniferous and younger taxa. It nests phylogenetically within a clade of post-Devonian species and, in an expanded phylogenetic analysis incorporating other previously neglected taxa, draws at least ten lineages of Carboniferous actinopterygians into the Late Devonian. This suggests phenotypically cryptic divergence among ray-finned fishes in the latest Devonian, followed by more conspicuous diversification in feeding and locomotor structures in the Carboniferous. Our revised model matches more complicated patterns of divergence, survival, and diversification around the Devonian-Carboniferous boundary in other vertebrate clades such as tetrapods and lungfishes. It also fundamentally recalibrates the onset of diversification early in the history of a group that today contains half of all living vertebrate species.

Main Text

Introduction

The compositional distinction between Devonian and Carboniferous vertebrate faunas has long been apparent (1, 2). Debate on the underlying cause of this faunal turnover focuses on whether it reflects a sudden transition stemming from mass extinction at the Devonian-Carboniferous boundary followed by explosive evolutionary recovery (3, 4), or a more gradual shift obscured by incomplete or understudied paleontological evidence (5, 6). Taken at face value, the fossil record of actinopterygians (ray-finned fishes) provides what appears to be strong evidence for more punctuated change mediated by the end-Devonian extinction, or Hangenberg Event. Actinopterygians persisted at low diversity (3) and abundance (7, 8) throughout the Devonian, but assumed their role as the dominant group of aquatic vertebrates in the early Carboniferous (3). Two important patterns of phenotypic change are associated with this taxonomic shift. First, Carboniferous actinopterygians show a significantly greater repertoire of body and skull shapes than their Devonian predecessors (9), including innovations for new modes of feeding (10, 11) and postcranial geometries indicative of novel locomotor modes (12). Second, there are indications of body-size reduction in actinopterygians and other vertebrate lineages at this time, interpreted as a protracted 'Lilliput effect' (13).

A rudimentary understanding of latest Devonian and earliest Carboniferous actinopterygians in conjunction with unstable phylogenetic relationships complicates interpretation of these apparent patterns. Consensus views on phylogeny indicate only one or two actinopterygian lineages crossed the Devonian-Carboniferous boundary (14-16) (but see (17)), suggesting that prolific diversity in the early Carboniferous arose through an explosive evolutionary radiation seeded by a handful of surviving groups, a mechanism historically proposed for famous examples like placental mammals (18). Recent analysis suggests variation on this theme, with an additional Devonian lineage persisting into the early Carboniferous alongside a single radiation containing all Carboniferous and younger taxa (19). Both of these models contrast with the emerging picture for other vertebrate survivors of the end-Devonian extinction: the cryptic early divergence of multiple lineages in the Late Devonian, followed by substantial ecomorphological radiation in the early Carboniferous. Inadequate taxonomic sampling in phylogenetic analyses of early actinopterygian relationships hinders meaningful discrimination among these three models.

Prevailing views of early actinopterygian evolution and diversification derive overwhelmingly from well-known taxa occurring millions of years before (20) or after (15, 21, 22) the Devonian-Carboniferous boundary. Deposits more proximate to the extinction event yield numerous taxa (23-26), but these are rarely included in systematic analyses because of a limited understanding of their anatomy stemming from their small size (25), incomplete preservation (26), or both. Fragmentary fossils from the latest Devonian (27) or earliest Carboniferous (19, 28) hint at a radically different interpretation of divergences before, survivorship across, and diversification after the end-Devonian extinction. Until the anatomy and relationships of these fossils is better resolved, their impact upon our understanding of actinopterygian evolution during this critical period remains, at best, suggestive.

Here we use micro-computed tomography to provide detailed anatomical information for a diminutive actinopterygian from the Late Devonian (middle Famennian; ca. 367 Ma) of the Appalachian Basin of the eastern United States. Previously referred to the problematic genus *Rhadinichthys* (29), it represents a new genus and species bearing an unexpected combination of derived features previously known only in Carboniferous and younger actinopterygians. This taxon prompts a reconsideration of trait evolution and tree topology that together provide evidence that numerous lineages of ray-finned fishes radiated before the end-Devonian mass extinction. This new perspective on ray-finned fish evolution complements

evidence in other groups for cryptic diversification before, and potentially high survivorship during, ecological crises at the end of the Devonian (30-35).

Systematic Paleontology

[redacted from preprint]

Diagnosis. Actinopterygian characterized by the following combination of characters: ornament comprising broad ridges incised with narrow grooves; dermosphenotic with well-developed posterior ramus; three suborbitals; ramifying tubules of infraorbital canals in jugal; separate braincase ossifications; median perforation in aortic canal of basicranium; two accessory vomers; dermal basipterygoid process; dermohyal unfused to imperforate hyomandibula.

Holotype. MCZ VPF 5114, a nearly complete fish preserved in part and counterpart, missing snout, anterior portion of lower jaw, and caudal fin (Fig. 1B, Fig. S6).

Horizon and locality. "Chemung" of Warren, Pennsylvania, USA (29). The Chemung of earlier workers is a facies rather than formal stratigraphic unit, represented in the Chadakoin and Canadaway formations in western Pennsylvania (36, 37). Only the younger of these, the Chadakoin Formation, is present in the collection locality (36). The Chadakoin Formation lies within the *Palmatolepis marginifera* Conodont Zone (Kirchgasser), Goniatite Zone II-G (38), and Fa2c subdivision of Spore Zone GF (39), indicating a mid-Famennian age, providing a constraint of 367.9-367.2 Ma for MCZ VPF 5114 (40). Other fishes reported from the Chadakoin Formation include arthrodire placoderms, chondrichthyans, lungfishes, and porolepiforms (29, 41).

Remarks. Eastman (29) referred MCZ VPF 5114 to the problematic genus *Rhadinichthys*, leaving it in open nomenclature as *Rhadinichthys* sp. Species assigned to *Rhadinichthys* do not form a clade (14), and the holotype of the type species, *R. ornatissmimus*, is poorly preserved (National Museum of Scotland NMS G.1878.18.7). There is no evidence linking MCZ VPF 5114 to this taxon to the exclusion of other early actinopterygians. The small size and incomplete endoskeletal ossification of this specimen may indicate that it is a juvenile.

Results

Skull roof. The skull roof comprises frontals, parietals, supratemporals and intertemporals (Fig. 2A, Fig. S1A-D, S2A,D). The frontal (fr; Fig. S2A-D) is the largest bone of the skull roof, and is approximately twice the length of the parietal. A midline suture between right and left frontals is not visible in CT scans, and it is unclear whether these bones were tightly joined or fused as a single plate. The lateral margin of the frontal is modestly stepped at mid-length, forming an inset to accommodate the supratemporal. A pineal foramen (pi; Fig S2B,C, Fig. S3D) pierces the midline of the skull roof within the frontal(s), the anterior margin of which is incomplete. The supraorbital canal (soc; Fig. S1A; Fig. S2A-D, Fig. S3A,D), marked by a thickening on the ventral surface of the bone, extends through the frontal and into the parietal. This canal is fully floored with bone anteriorly but is open ventrally posterior to the level of the pineal foramen. The paired parietals (pa; Fig. S2B-D, Fig. S3D) are quadrate in shape, and a short posterior extension of the supraorbital canal appears as a faint ridge on the outer surface of the bone with a matching groove on its ventral surface. The dorsal surface of the parietal bears posterior (ppl; Fig. S2C) and middle (mpl; Fig. S2C) pit-lines. A modest intertemporal (it; Fig. 2A, Fig. S1A, Fig. S2A,C, Fig. S3A) lies entirely anterior to the suture between the parietal and frontal. It carries a short segment of the infraorbital canal (ioc; Fig. S1A, Fig. S2C,D, Fig. S3A,B) along its thickened ventrolateral margin. The lenticular supratemporal (st; Fig. 2A, Fig. S1A, Fig S2A-D; Fig. S3A) is very long, extending from behind the posterior margin of the parietal to halfway along the frontal. The infraorbital canal is carried in a thickened ridge on the inner surface of the bone along its lateral margin. The lateral margin of the

supratemporal abuts the preoperculum, and posterior to this contact a branch of the infraorbital canal extends toward the preopercular canal to form a jugal canal (jgc; Fig. S1A).

Cheek. The cheek comprises a dermosphenotic, jugal, lacrimal, three suborbitals, and preoperculum (Fig. 2A, Fig. S1A-D, S2A,B,D). The dermosphenotic (dsph; Fig. 13A, Fig. S1A, Fig. S2A,C; Fig. S3A) is 'T'-shaped, with long anterior and posterior limbs and a short ventral limb. The infraorbital canal extends through the ventral limb of the bone into the jugal, and a branch in the anterior limb of the dermosphenotic approaches but does not connect with the supraorbital canal of the frontal. Within the jugal (jug; Fig. 2A, Fig. S1A, Fig. S2A; Fig. S3A), the canal extends in a thickened ridge visible on the inner surface of the bone offset from the orbital margin. At least 14 branches of the infraorbital canal (ram; Fig. 3A, Fig. S1a, Fig. S3A,B) radiate into the posterior portion of the jugal. The lacrimal (lac; Fig. S2A-D, Fig. S3A) is formed as a tube of bone transmitting the infraorbital canal. Three suborbitals (sorb; Fig. 2A, Fig. 3A, Fig. S1A, Fig. S2A, Fig. S3A,B) lie in the space between the dorsal limb of the jugal and the anterior margin of the preoperculum. They are arranged in a vertical series, with the middle suborbital smaller than the dorsal and ventral ones. The preoperculum (pop; Fig. S2A) is boomerang-shaped, with an anterior limb broader than the ventral limb. The angle between these limbs bears a broad overlap area for the maxilla. The preopercular canal (popc; Fig. S1A) extends in a thickened ridge on the inner surface of the bone, near its dorsal margin. Two pit-lines form an inverted 'V' (popl; Fig. S1A) at the angle between the two limbs of the preoperculum. The presence of a quadratojugal is uncertain.

Upper jaw and palate. Preserved components of the upper jaw include the maxilla, a putative premaxilla, the quadrate and the dermal palatal bones (Fig. 2A,B, Fig. S2C,F,G).The cleaver-shaped maxilla (mx; Fig. 2A,B, Fig. S1A,B, Fig. S2A,D, Fig. S3F) has a broad, high posterior plate, and a narrow, gently curved suborbital limb. The posterior margin of the bone is very thin, petering out to nothing within the scan data, and its true margin is difficult to discern. A posteroventral extension of the posterior plate (ov; Fig. S3F) overlaps the lower jaw. A narrow shelf (sh; Fig. S3F) extends along the medial surface of the bone, beginning at the tip of the suborbital limb and continuing to the point at which the posterior plate overlaps the lower jaw. Ornament on the maxilla comprises a series of broad, flat ridges that are only narrowly separated from each other, resembling a plateau of enamel separated by narrow grooves. Maxillary teeth are arranged in a row along the ventral margin of the bone, but only sockets are preserved. Marginal teeth are not visible, but it is unclear if this represents true absence or a limit to scan resolution. An elongate, narrow strip of dermal tooth-bearing bone medial to the maxilla may represent a displaced premaxilla (?pmx; Fig. S3C).

The endoskeletal portion of the palate is largely unmineralized. The quadrate (qu; Fig. 2B, Fig. S1B, Fig. S3G) is well-ossified, with two prominent condyles. Apart from this, mineralization of the palatoquadrate is restricted to a short narrow strip extending from the quadrate along the presumed posterodorsal margin of the cartilage. The dermal ossifications of the palate are preserved as separate bones, but divisions between them are not always clear. The ectopterygoid (ectp; Fig. 2B, Fig. S1B) is long and ovoid, with an irregular anterior margin but narrowing to a point near the quadrate posteriorly. Dorsally, it is bordered by at least three separately ossified dermatopterygoids (dmpt; Fig. 2B, Fig. S1B), although a gap between two of these ossifications suggests four were likely present in total. Ventral to the entopterygoid, the demopalatines presumably form a long narrow extension continuous with the ectopterygoid, although as sutures are not visible between these in the scan data their exact number cannot be determined. The entopterygoid (entp; Fig. 2B; Fig. S1B), which is roughly rectangular, lies dorsal to the anterior half of the demopalatine series.

There are two accessory vomers (av; Fig. 2B, Fig. S1B, Fig. S4B) on each side of the skull, closely associated with the parasphenoid. The anterior accessory vomer is approximately twice the length of the posterior one, and tapers slightly toward its anterior end. The anterior accessory vomer is confined anterior to the basipterygoid process, while the posterior accessory vomer traces the spiracular groove on

the ascending process of the parasphenoid. The anterior accessory vomer broadly overlaps the anterior corpus of the parasphenoid.

Lower jaw. The lower jaw is incomplete anteriorly but comprises dermal components of the outer and inner surface and the articular (Fig. 2A,B, Fig. S2E-G). The external surface of the lower jaw includes a dentary (dent; Fig. 2A,B, Fig. S1A,B, Fig. S2A,B,D,E, Fig. S3E,F) and at least one postdentary bone (ang; Fig. 2B, Fig. S1B, Fig. S3E,F). A semicircular depression floored with very thin bone (which is too thin to segment) marks the posterodorsal portion of the dentary, and represents the overlap area for the maxilla. Ornament on the dentary resembles that of the maxilla. The mandibular canal (mc; Fig. S1A,B, Fig. S3F) traverses the ventral margin of the dentary and the posteroventral margin of the postdentary; this thickened portion is the only part of the postdentary thick enough to be visualized from the scan, although the suture between the dentary and postdentary is visible externally. A single row of seven large conical teeth (t; Fig. 2B, Fig. S1B, Fig. S3F) is present along the dorsal margin of the dentary, with at least seven additional empty sockets preserved in this row. No smaller secondary row of dentition is visible lateral to these teeth, although any marginal dentition may be beyond the resolution of the scans.

The mesial surface of the lower jaw is covered by dermal bone, probably representing the prearticular and coronoids (part; Fig. 2B, Fig. S1B, Fig. S2B,E, Fig. S3E,G), although divisions between bones are indistinct. This complex defines the mesial margin of the adductor fossa (add; Fig. S3E) posteriorly, and narrows anteriorly. A longitudinal ridge (ri; Fig. S3E,G) is present on the dorsal surface of these dermal bones. No distinct teeth are visible, but it is possible that small denticles were present, suggested by modest crenulation of this ridge. Irregularly shaped toothplates (tp; Fig. 2B, Fig. S1B; Fig. S3G) are applied to the exposed mesial surface of the prearticular/coronoid complex anterior to the adductor fossa. Three toothplates are present on each mandible. Narrow gaps separate individual toothplates, which collectively form a large elliptical composite plate.

Only the articular region (art; Fig. 2B, Fig. S1B, Fig. S3E,G) of Meckel's cartilage is ossified. It bears two concave facets, one mesial and one lateral, that match the convex condyles on the quadrate.

Neurocranium and parasphenoid. The braincase is only partially ossified, and is floored by a short parasphenoid (Fig. 2D, Fig. S1B,D, Fig. S3A-C). Mineralization of the neurocranium is largely restricted to the otic and occipital region, comprising by a basioccipital plate (boc; Fig. S4A,B); dorsal, paired ossifications corresponding to the exoccipital components of the occipital arch (exo; Fig. 2D, Fig. S1D, Fig. S4A-C); paired, nodular ossifications anterior to the exoccipitals possibly representing intercalars (?ic; Fig. 2D, Fig. S1D, Fig. S4A-C), and a small ossification posterodorsal to the orbit in the sphenotic region (sph; Fig. 2D, Fig. S1D, Fig. S4A-C). A well-developed aortic canal (aoc; Fig. S4A,B) extends the length of the basioccipital ossification. A prominent midline foramen for the efferent artery (epi.a; Fig. 3B, Fig. S4B) pierces the floor of the canal in its posterior third. The exoccipital ossifications preserve few details apart from a single foramen on their lateral surfaces, possibly for a spinoccipital nerve.

The parasphenoid (psp; Fig. 2D, Fig. S1D, Fig. S4A-C) comprises a plank-like anterior corpus and a short posterior extension with a rounded margin. Because of the lack of endocranial mineralization, it is unclear if this posterior process bridged a ventral fissure. In cross-section, the anterior corpus is concave ventrally and convex dorsally. A broad, rounded ridge extends along the dorsal midline of the anterior half of the corpus, while a narrow, denticulated ridge extends the length of the corpus on the ventral surface of the bone. This ventral ridge represents the portion of the corpus exposed when the accessory vomers are in articulation. Three major structures are present near the junction between the anterior corpus and posterior extension of the parasphenoid: a prominent buccohypophysial foramen (bhc; Fig. S4B) along the midline, and modest dermal basipterygoid processes (d.bpt; Fig. 3B, Fig. S4B) and long ascending processes (asp; Fig. 2D, Fig. S1D, Fig. S4A-C) extending from the lateral margin of the bone. Deep notches mark the posterior intersection of the ascending processes and the body of the parasphenoid,

but do not pierce the corpus. A parabasal canal is present. Pronounced spiracular grooves (spig; Fig. S4A) extend along the lateral surfaces of the ascending processes.

Hyoid arch and associated dermal bones. Endoskeletal ossifications of the hyoid arch include the hyomandibula and ceratohyal, both of which are incompletely mineralized (Fig. 2D, Fig. S1B, 3C-D). These are joined by a large dermohyal. The imperforate hyomandibula (hmd; Fig. 2D, Fig. S1D, Fig. S2B-E, Fig. S4C,D) has a distinct elbow marking the junction of its dorsal and ventral limbs, but no opercular process is present. A groove on the dorsomedial surface of the upper limb marks the course of the hyomandibular branch of the facial nerve. Mineralization of the hyomandibula is incomplete proximally and distally. The plate-like ceratohyal (chy; Fig. 2D, Fig. S1D, Fig. S2A,B,D,E, Fig. S4C,D) lacks a medial constriction and bears a lateral groove on its dorsal third that marks the course of the afferent hyoid artery (ahy; Fig. S4D). The proximal and distal ends of the bone are unmineralized. Only the right ceratohyal is completely enclosed in rock, with the left bone partially exposed on the surface at a break in the specimen. The triangular dermohyal (dhy; Fig. 3C, Fig. S4D) is longer than the preserved dorsal shank of the hyomandibula, and the two are unfused.

Branchial arches. Mineralization of the gill skeleton is generally poor throughout (Fig. 2D, Fig. S1B,D, Fig. S3C-F). The gill skeleton has four rod-like ceratobranchials (cb; Fig. 2D, Fig. S1D, Fig. S2E, Fig. S4C,E,F) bearing a longitudinal ventral groove, with a poorly mineralized and narrow fifth arch visible in the scan but beyond the limit of segmentation. Paired bones representing hypobranchial 1 (hb; Fig. S2A,B,D, Fig S4C,E,F) lie at the anterior of the gill skeleton, but are displaced from life position. Hypobranchial 1 is one third the length of ceratobranchial 1, and has a ventral process at its proximal end. The basibranchial (bb; Fig. S4E,F) is largely unossified, but a small segment bearing paired swellings is preserved anterior to the second ceratobranchials.

The dorsal gill skeleton is less complete. Two epibranchials (eb; Fig. 2D, Fig. S1D, Fig. S2B,D, Fig. S4C,E-F) are mineralized on each side of the skull. Each bears a dorsal longitudinal groove and an uncinate process (unc; Fig. 3D, Fig. S1D). A single pharyngobranchial (pb; Fig. S4E) is preserved on each side of the specimen, in articulation with the basioccipital.

Operculogular series. The operculogular series comprises an operculum, suboperculum, and branchiostegals (Fig 2A, Fig. S1A,B). The operculum (op; Fig. 2A, Fig. S1A, Fig. S2A,B) is rhombic in outline, with a long diagonal axis. Ridges ornament the external surface of the bone, which bears a small prong at its anterior corner. The quadrangular suboperculum (sop Fig. 2A, Fig. S1A, Fig. S2A,B,E) is half the size of the operculum. At least 12 or 13 splint-shaped branchiostegals (br; Fig. 2A, Fig. S1A, Fig. S2A,D,E) are preserved. The most posterior branchiostegal is the deepest, with more anterior members of the series narrower. As the anteriormost branchiostegals are exposed on the surface, and it is not possible to determine their exact number or the condition of any gular plates.

Pectoral girdle and fin. The dermal shoulder girdle includes extrascapulars, a posttemporal, presupracleithrum, supracleithrum, cleithrum, and clavicle (Fig. 2A,C, Fig. S1, Fig. S4). As only one half of the skull roof is preserved, the exact number of extrascapulars (exsc; Fig. S2A,C,D) is unknown, but it seems likely that only one bone was present per side. There is no trace of a medial branch of a lateral line canal in the extratemporal, although aligned canals are clearly preserved anterior and posterior to bone on the visceral surfaces of the parietal and posttemporal. The leaf-shaped posttemporal (pt; Fig. S2A-D) makes a broad contact with the extrascapular(s), and overlaps the presupracleithrum (pscl; Fig. S2A) laterally and supracleithrum (sclth; Fig. S2A-D) posterolaterally. A pronounced groove is visible for the lateral line (ll; Fig. 2A, Fig. S1A, Fig. S2A,B) on the external face of the large supracleithrum. The cleithrum (clth; Fig. 2C, Fig. S1C, Fig. S2A,B,E, Fig. S5A,C-E) is broad, with both a laterally-directed and medially-directed face, both bearing long ridges of ornament. These two faces are separated on the medial face of the cleithrum by a deep ridge, which gets narrower and shallower ventrally. Anterior to the cleithra are paired clavicles (clav; Fig. 2C, Fig. S1C, Fig, S2A,D,E, Fig. S5A,C-F), which narrowly overlap

the anterior face of the cleithra. The anterodorsal portion of the clavicle is developed as a long, narrow spine extending along the anterodorsal margin of the cleithrum. The clavicles are strongly curved, with dorsal and ventral faces ornamented with long ridges. Between the dermal shoulder girdles lies an elongate, arrow-shaped interclavicle (icl; Fig. 2C, Fig. S1C, Fig. S5AC,D), which ends in a narrow point anteriorly. The ventral surface of the interclavicle is developed as a narrow ridge, which would have been exposed between the ventral faces of the clavicles.

The endoskeletal shoulder girdle is well ossified. Rather than being a single triradiate ossification, the scapulocoracoid is present as several separate ossifications. The largest is portion is a curved, horizontal ossification (scpc.hz; Fig. S5C-F), the lateral face of which abuts the cleithrum and the posterior face of which contacts the propterygium. The remaining radials were presumably supported by a posterior cartilaginous extension of the endoskeletal girdle. Three flat, curved plates (scpc.pl; Fig. S5C,D), each smaller and narrower than the horizontal portion, comprise the remainder of the scapulocoracoid, but do not appear to be in life position. Three stout and rod-like radials (rad; Fig. 2C, Fig. S1C, Fig. S5A-C,E,G,H) are present between the metapterygium and propterygium. The propterygium (ptg; Fig. S5B,C,E,G,H) is more complex in shape, more than twice the size of any other radial and pierced by the propterygial canal (ptg.ca; Fig. S5G,H). The metapterygium (mptg; Fig. S5B,C,G,H) is longer than the remaining radials and supports one preaxial radial (pr.rad; Fig. S5B,E,G,H).

At least three proximate lepidotrichs are fused together at the leading edge of the fin (fu; Fig. S5A-C), although they do not appear to embrace the propterygium. The remaining lepidotrichs (lep; Fig. 2C, Fig. S1C, Fig. S2A,B, Fig. S5A-C,E) of the pectoral fin are evenly segmented and appear to bifurcate distally. Fringing fulcra are absent.

Little of the remaining fins can be described. There are no basal scutes preceding fins. The anal fin appears to bear fringing fulcra, and pelvic fins are present.

Scales. The scales are rhombic, with a ridge on the internal surface. They articulate via a narrow peg and socket (Fig. 2A, Fig.S2F). Ornament on the scales is broadly similar to that on the body, comprising broad flat ridges of enamel incised with roughly parallel narrow grooves.

Discussion

Anatomical comparisons and phylogenetic placement.

The combination of characters displayed by MCZ VPF 5114 [new taxon name redacted from preprint] is unexpected. While externally unremarkable, our CT data reveal internal anatomy unanticipated in a Devonian actinopterygian (Fig.34A-C). Most prominent is the presence of a midline perforation in the aortic canal and the presence of dermal basipterygoid processes, both previously known only in post-Devonian taxa (22, 42-45). This is joined by features such as suborbitals and multiple rami of the infraorbital canal in the jugal that are only sporadically reported in Devonian species (e.g. *Moythomasia nitida* (46, 47); *Moythomasia lineata*: (46, 47); Fig 3D-F) but overwhelmingly present in Carboniferous and younger taxa (Fig 3H-J). The size of MCZ VPF 5114 [new taxon name redacted from preprint] is small, but not exceptionally so (total length approximately 50 mm). Some aspects of its anatomy are consistent with an earlier ontogenetic stage (e.g., separate ossifications of the neurocranium and palatoquadrate), but the features that ally it with Carboniferous actinopterygians do not appear to reflect transient juvenile features based on development in extant species (48, 49).

This qualitative assessment is corroborated by formal phylogenetic analysis of an expanded published matrix (50) to incorporate additional Famennian (n = 8) and Tournaisian (n = 5) actinopterygians. Both our parsimony (Fig. S7) and Bayesian analyses (Fig. S8) recover MCZ VPF 5114 [new taxon name redacted from preprint] as a stem actinopterygian in an immediate clade with two Mississippian taxa (*Cyranorhis bergeraci* and *Wendyichthys dicksoni*). In common with previous analyses (16, 50), resolution is poor

across the Bayesian tree. In our parsimony analysis, MCZ VPF 5114 [new taxon name redacted from preprint] and its sister taxa are recovered in a broader clade of Carboniferous–Triassic ray-finned fishes. The Serpukhovian *Woodichthys* is recovered as the sister taxon to this clade, which branches from a polytomy that also includes *Melanecta*, a clade comprising *Saurichthys*, amphicentrids+styracopterids, and a lineage leading to the actinopterygian crown. The placement of MCZ VPF 5114 [new taxon name redacted from preprint] as nested within a Carboniferous radiation is supported by characters relating to the dermal and endoskeleton (Dataset S5).

A detailed picture of relationships amongst other Devonian taxa is unclear, but we recover additional clades that comprise both Devonian and stratigraphically younger forms. This contrasts with the majority of recent phylogenetic hypotheses, which generally recover all post-Devonian taxa in just one (16, 50) or two (14, 15, 20, 51) clades. Earlier analyses suggesting more substantial diversification outside of the actinopterygian crown (17, 52) are likely biased by methodological and sampling issues (53). MCZ VPF 5114 [new taxon name redacted from preprint] establishes that key anatomical features previously thought restricted to Carboniferous and younger taxa arose in the Devonian. The nested phylogenetic position of MCZ VPF 5114 [new taxon name redacted from preprint] and some other Late Devonian taxa in our analyses provides explicit support for the hypothesis that numerous actinopterygian lineages crossed the end-Devonian boundary.

Models of early actinopterygian diversification.

Timing of divergences among early actinopterygians in past studies is either taken at face-value from the fossil record (3, 13) or depicted graphically in trees (19, 54, 55) timescaled using naïve *a posteriori* approaches that impose user-defined branch minima or redistribute branch lengths among clades (56). Prevailing hypotheses using these approaches posit that a minimal number of lineages crossed the end-Devonian boundary, with explosive diversification occurring in the early Carboniferous. A minor modification of this hypothesis suggests that the Devonian moythomasiid clade survived the extinction, persisting for a short time alongside the Carboniferous radiation. Even without formal analysis of divergence times, our placement of MCZ VPF 5114 [new taxon name redacted from preprint] instead supports a third model: previously unrecognised diversification in the Late Devonian that led directly to the post-extinction radiation.

A fossil birth-death analysis (57) provides a more explicit timescale for early actinopterygian evolution (Fig. 4; Fig. S9; Dataset S4), and places the origin of crown actinopterygians in the Late Devonian or earliest Carboniferous (mean: 364.4 MA [million years ago]; 95% highest posterior density: 379.1 MA–351.6 MA). The maximum clade credibility tree suggests that at least ten lineages—an order of magnitude more than inferred by most recent analyses (16, 50)—persisted into the Carboniferous, indicating substantial and hitherto cryptic diversification before the end-Devonian extinction. The significance of internal anatomy in placing fossils, combined with the small size of many Late Devonian taxa, likely accounts for past failures to recognize this pattern.

Body size is an important correlate of many aspects of life history and ecology, with many questions centering on impacts on body size during intervals of biotic crisis. Across all marine groups, selectivity on body size is more conspicuous during mass extinctions and their recovery intervals (58). Decreases of mean body size associated with the Devonian-Carbonferous boundary have previously been reported in many vertebrate clades, including actinopterygians (13). Our dataset provides a phylogenetically informed assessment of this pattern. While we find a general decrease in body size from the latest Devonian into the early Carboniferous, there is no strong inflection close to the boundary itself (Fig. 5B), and an interrogation of size distribution in boundary-crossing lineages suggests that most were mid-sized (Fig. 5A). More densely sampled phylogenetic hypotheses will be necessary for assessing impacts of the biotic turnover during the Devonian/Carboniferous extinction on the trajectory of body-size evolution in ray-finned fishes.

Importantly, the features that nest MCZ VPF 5114 [new taxon name redacted from preprint] and some other Late Devonian taxa within clades composed mostly of younger taxa relate to relatively minor aspects of anatomy, rather than the substantial mandibular and locomotor innovations interpreted as evidence of increased ecological diversity among Carboniferous taxa (9-11, 28). Thus, the initial diversification of actinopterygians appears to show decoupling of cladogenetic events, which took place prior to the end-Devonian extinction, from subsequent ecomorphological and trophic divergence, which took place in the early Carboniferous. Such offsets between lineage divergence and phenotypic diversification are a common feature of vertebrate evolution (59, 60). A similar pattern also seems to characterize the radiation of placental mammals, where a growing consensus places many intra-ordinal divergences in the Late Cretaceous with the emergence of ecologically distinct radiations in the Cenozoic following the end-Cretaceous extinction (61, 62). Evidence suggests this might be a common evolutionary trajectory for vertebrate lineages across the Devonian-Carboniferous boundary, with both tetrapods and lungfishes showing substantial lineage diversification before, and morphological divergence after, the extinction (30-35).

Materials and Methods

CT scanning. MCZ (Harvard Museum of Comparative Zoology) VPF 5114 was scanned on a Nikon XT 225 ST micro CT scanner at the CTEES facility, Department of Earth and Environmental Sciences, University of Michigan. Details of the scan: voltage = 130 kV; current = 115 μA; exposure = 4 s; frames per projection = 2; projections = 3141; filter = 1 mm Cu. After scanning, data were segmented in Mimics (http://biomedical.materialise.com/mimics; Materialise, Leuven, Belgium). Surface meshes were then exported into and imaged in Blender (http://blender. org; Stitching Blender Foundation, Amsterdam, the Netherlands). The raw projection series, reconstructed .TIFF stack, and .OBJ file of all segmented 3D objects are available on Morphosource.org (https://www.morphosource.org/concern/biological_specimens/000417029). During the review process, the Mimics file can be downloaded upon request from the Department of Vertebrate Paleontology at the Museum of Comparative Zoology; the identities of anyone who downloads the data, including reviewers, will not be made available to the authors of the paper.

Phylogenetic analysis. Analyses were performed in TNT v1.5 (63) and MrBayes v.3.2.6 (64) using a dataset modified from Latimer & Giles (50) and Figueroa et al. (65) with the addition of ten taxa, giving a total of 121 taxa and 292 characters. Full details are given in the Supplementary Information. An equally weighted parsimony analysis was conducted in TNT using the following settings: hold 200000; xmult=level10; bbreak=fillonly. The outgroup was set as *Dicksonoteus arcticus*, and the following topology constraint was applied: [*Dicksonosteus* [*Entelognathus* [*Acanthodes*, *Cladodoides*, *Ozarcus*][ingroup]]]. Bremer decay values were calculated in TNT, and an agreement subtree was calculated in PAUP* 4.0a169 (66). We conducted a Bayesian analysis with no stratigraphic information and identical constraints on outgroup taxa, discarding the first third of the run as burnin. To infer the timescale of early actinopterygian diversification, we also conducted an additional Bayesian analysis under the fossil-birth-death (FBD) prior. Taxa were assigned uniform age priors matching the duration of the shortest temporal interval to which they could be assigned (e.g., conodont or ammonoid zones for many Devonian-Carboniferous taxa). In the absence of meaningful prior estimates of key parameters like preservation, extinction, and speciation rates, we adopted uninformative priors suggested by Matzke & Wright (67). In addition to constraints among non-osteichthyans, we applied a topological constraint for osteichthyan interrelationships matching the strict consensus from parsimony analyses. Analyses were run for a total of 6,000,000 generations, with two chains.

Acknowledgments

We thank the Harvard Museum of Comparative Zoology for specimen access and especially Jessica Cundiff for organizing the loan of material that formed the basis of this study. We also thank Emma Bernard, David Gelsthorpe, Zerina Johanson, Lindsay Loughtman, Paul Shephard and Stig Walsh for facilitating access to comparative collections; Graeme Lloyd for helpful discussions; and Christina Byrd for assistance with data archiving. SG was supported by a Royal Society Dorothy Hodgkin Research Fellowship (DH160098). This study includes data produced in the CTEES facility at University of Michigan, supported by the Department of Earth and Environmental Sciences and College of Literature, Science, and the Arts.

Author Contributions: MF and SP designed research; SG, MF, KF and RW performed research and analysed data; SG and MF wrote the paper and designed figures; all authors edited text.

Competing Interest Statement: The authors declare no competing interests.

References

1. A. S. Woodward, *Catalogue of the Fossil Fishes in the British Museum (Natural History). Part II. Containing the Elasmobranchii (Acanthodii), Holocephali, Ichthyodorulites, Ostracodermi, Dipnoi, and Teleostomi (Crossopterygii and Chondrostean Actinopterygii)* (Trustees of the British Museum (Natural History), London, 1881), pp. 567.
2. A. S. Woodward, *Catalogue of the Fossil Fishes in the British Museum (Natural History). Part III. Containing the Actinopterygian Teleostomi of the Orders Chondrostei (Concluded), Protospondyli, Aethospondyli, and Isospondyli (In Part)* (Trustees of the British Museum, London, 1895).
3. L. C. Sallan, M. I. Coates, End-Devonian extinction and a bottleneck in the early evolution of modern jawed vertebrates. *Proceedings of the National Academy of Sciences of the USA* **107**, 10131-10135 (2010).
4. T. R. Smithson, K. R. Richards, J. A. Clack, Lungfish diversity in Romer's Gap: reaction to the end-Devonian extinction. *Palaeontology* **59**, 29-44 (2016).
5. J. S. Anderson, T. R. Smithson, C. F. Masksy, T. Meyer, J. A. Clack, A diverse tetrapod fauna from the base of 'Romer's Gap'. *PLoS ONE* **10**, e0125446 (2015).
6. T. R. Smithson, S. P. Wood, J. E. A. Marshall, J. A. Clack, Earliest Carboniferous tetrapod and arthropod faunas populate Romer's Gap. *Proceedings of the National Academy of Sciences of the USA* **109**, 4532-4537 (2012).
7. J. A. Long, K. Trinajstic, The Late Devonian Gogo Formation Lägerstatte of Western Australia: Exceptional Early Vertebrate Preservation and Diversity. *Annual Reivew of Earth and Planetary Sciences* **38**, 255-279 (2010).
8. N. H. Trewin, Palaeoecology and sedimentology of the Achanarras fish bed of the Middle Old Red Sandstone, Scotland. *Transactions of the Royal Society of Edinburgh: Earth Sciences* **77**, 21-46 (1986).
9. L. C. Sallan, M. Friedman, Heads or tails: staged diversification in vertebrate evolutionary radiations. *Proceedings of the Royal Society B* **279**, 2025-2032 (2012).
10. M. Friedman, S. E. Pierce, M. I. Coates, S. Giles, Feeding structures in the ray-finned fish *Eurynotus crenatus* (Actinopterygii: Eurynotiformes): implications for trophic diversification among Carboniferous actinopterygians. *Earth and Environmental Science Transactions of the Royal Society of Edinburgh* **109**, 33-47 (2019).

11. L. C. Sallan, M. I. Coates, Styracopterid (Actinopterygii) ontogeny and the multiple origins of post-Hangenberg deep-bodied fishes. *Zoological Journal of the Linnean Society* **169**, 156-199 (2013).
12. L. Sallan, Tetrapod-like axial regionalization in an early ray-finned fish. *Proceedings of the Royal Society B* **279**, 3264-3271 (2012).
13. L. C. Sallan, A. K. Galimberti, Body-size reduction in vertebrates following the end-Devonian mass extinction. *Science* **350**, 812-815 (2015).
14. B. G. Gardiner, B. Schaeffer, Interrelationships of lower actinopterygian fishes. *Zoological Journal of the Linnean Society* **97**, 135-187 (1989).
15. M. I. Coates, Endocranial preservation of a Carboniferous actinopterygian from Lancashire, UK, and the interrelationships of primitive actinopterygians. *Philosophical Transactions of the Royal Society B* **354**, 435-462 (1999).
16. S. Giles, G.-H. Xu, T. J. Near, M. Friedman, Early members of a 'living fossil' lineage imply later origin of modern ray-finned fishes. *Nature* **549**, 265-268 (2017).
17. R. Cloutier, G. Arraita, "Early diversification of actinopterygians" in Recent Advances in the Origin and Early Radiation of Vertebrates*,* G. Arratia, M. V. H. Wilson, R. Cloutier, Eds. (Verlag Dr. Friedrich Pfeil, Munich, 2004), pp. 217-270.
18. M. A. O'Leary *et al.*, The placental mammal ancestor and the post-K-Pg radiation of placentals. *Science* **339**, 662-667 (2013).
19. C. D. Wilson, J. D. Pardo, J. S. Anderson, A primtive actinopterygian braincase from the Tournaisian of Nova Scotia. *Royal Society Open Science* **5**, 171727 (2018).
20. B. G. Gardiner, The relationships of the palaeoniscid fishes, a review based on new species of *Mimia* and *Moythomasia* from the Upper Devonian of Western Australia. *Bulletin of the British Museum (Natural History) Geology* **37**, 173-428 (1984).
21. M. I. Coates, Actinoptergians from the Namurian of Bearsden, Scotland, with comments on early actinopterygian neurocrania. *Zoological Journal of the Linnean Society* **122**, 27-59 (1998).
22. C. Poplin, *Étude de quelques paléoniscidés pennsylvaniens du Kansas*, Cahier de Paléontologie (Éditions du CNRS, Paris, 1974).
23. D. H. Dunkle, Preliminary description of a paleoniscoid fish from the Upper Devonian of Ohio. *Scientific Publications of the Cleveland Museum of Natural History, New Series* **3**, 1-16 (1964).
24. M. Friedman, H. Blom, A new actinopterygian from the Famennian of East Greenland and the interrelationships of Devonian ray-finned fishes. *Journal of Paleontology*, 1186-1204 (2006).
25. E. B. Daeschler, An early actinopterygian fish from the Catskill Formation (Late Devonian, Famennian) in Pennsylvania, U.S.A. *Proceedings of the Academy of Natural Sciences of Philadelphia* **150**, 181-192 (2000).
26. A. M. Prokofiev, First finding of an articulated actinopterygian skeleton from the Upper Devonian of Siberia and a reappraisal of the family Moythomasiidae Kazantseva, 1971 (Osteichthyes). *Paleontological Research* **6**, 321-327 (2002).
27. P. Janvier, F. Lethiers, O. Monod, Ö. Balkas, Discovery of a vertebrate fauna at the Devonian-Carboniferous boundary in SE Turkey (Hakkari Province). *Journal of Petroleum Geology* **7**, 147-168 (1984).
28. C. D. Wilson, C. F. Mansky, J. S. Anderson, A platysomid occurrence from the Tournaisian of Nova Scotia. *Scientific Reports* **11.1**, 1-12 (2021).
29. C. R. Eastman, *Devonic Fishes of the New York Formations*, Memoirs of the New York State Museum (New York State Education Dept., Albany, 1907).

30. T. J. Challands *et al.*, A lungfish survivor of the end-Devonian extinction and an Early Carboniferous dipnoan radiation. *Journal of Systematic Palaeontology* 10.1080/14772019.2019.1572234 (2019).
31. J. A. Clack, T. J. Challands, T. R. Smithson, K. Z. Smithson, Newly recognized Famennian lungfishes from East Greenland reveal tooth plate diversity and blur the Devonian-Carboniferous boundary. *Papers in Palaeontology* **5**, 261-279 (2019).
32. J. S. Anderson, T. Smithson, C. F. Mansky, T. Meyer, J. A. Clack, A diverse tetrapod fauna at the base of 'Romer's Gap'. *PLoS ONE* **10**, e102446 (2015).
33. E. B. Daeschler, J. A. Clack, N. H. Shubin, Late Devonian tetrapod remains from Red Hill, Pennsylvania, USA: how much diversity? *Acta Zoologica* **90**, 306-317 (2009).
34. P. E. Ahlberg, J. A. Clack, The smallest known Devonian tetrapod shows unexpectedly derived features. *Royal Society Open Science* **7**, 192117 (2020).
35. J. D. Pardo, M. Szostakiwskyj, P. E. Ahlberg, J. S. Anderson, Hidden morphological diversity among early tetrapods. *Nature* **546**, 642-645 (2017).
36. Anonymous (1980) Geologic Map of Pennsylvania 1:250,000. ed A. A. Socolow (Commonwealth of Pennsylvania, Department of Environmental Resources).
37. P. Startenaer, *Jacoburbirostrum*, a new middle Famennian rhynchonellid (brachiopod) genus from southwestern New York State. *Bulletin of Geosciences* **89**, 607-616 (2014).
38. M. R. House, W. T. Kirchgasser, Late Devonian goniatites (Cephalopoda, Ammonoidea) from New York State. *Bulletins of American Paleontology* **374**, 1-285 (2008).
39. J. Clendening, A., L. E. Eames, G. D. Wood, *Retusotriletes phillipsii* n. sp., a potential Upper Devonian guide palynomorph. *Palynology* **4**, 15-21 (1980).
40. R. T. Becker, J. E. A. Marshall, A.-C. Da Silva, "The Devonian Period" in Geologic Time Scale 2020*,* F. M. Gradstein, J. G. Ogg, M. D. Schmitz, G. M. Ogg, Eds. (Elsevier, Amsterdam, 2020), pp. 733-810.
41. K. M. Yeager, Fossil fishes (Arthrodira and Acanthodida) from the Upper Devonian Chadokoin Formation of Erie County, Pennsylvania. *Ohio Journal of Science* **96**, 52-56 (1996).
42. D. H. Rayner, n the Cranial Structure of an Early Palæoniscid, Kentuckia, gen. nov. . *Transactions of the Royal Society of Edinburgh* **62**, 53-83 (1952).
43. M. H. Hamel, C. Poplin, The braincase anatomy of *Lawrenciella schaefferi*, actinopterygian from the Upper Carboniferous of Kansas (USA). *Journal of Vertebrate Paleontology* **28**, 989-1006 (2008).
44. B. Schaeffer, W. W. Dalquest, A palaeonisciform braincase from the Permian of Texas, with comments on cranial fissures and the posterior myodome. *American Museum Novitates* **2658**, 1-15 (1978).
45. E. Nielsen, Studies on Triassic fishes I. *Meddelelser om Grønland* **138**, 1-394 (1942).
46. H. Jessen, *Moythomasia nitida* Gross und *M*. cf. *striata* Gross, Devonische Palaeonisciden aus dem oberen Plattenkalk der Bergisch-Gladbach-Paffrather Mulde (Rheinisches Schiefergebirge). *Palaeontographica Abteilung A* **128**, 87-114 (1968).
47. B. Choo, A new species of the Devonian actinopterygian *Moythomasia* from Bergisch Gladbach, Germany, and fresh observations on *M. durgaringa* from the Gogo Formation of Western Australia. *Journal of Vertebrate Paleontology* **35**, e952817 (2015).
48. J. A. Moy-Thomas, Memoirs: notes on the development of the chondrocranium in *Polypterus senegalus*. *Journal of Cell Science* **(2) 76**, 209-229 (1933).
49. J. Daget, M. L. Bauchot, R. Bauchot, J. Arnoult, Développement du chondrocrâne et des arcs aortiques chez Polypterus senegalus Cuvier. *Acta Zoologica* **45**, 201-244 (1964).

50. A. E. Latimer, S. Giles, A giant dapediid from the Late Triassic of Switzerland and insights into neopterygian phylogeny. *Royal Society Open Science* **5**, 180497 (2018).
51. B. G. Gardiner, B. Schaeffer, J. A. Masserie, A review of the lower actinopterygian phylogeny. *Zoological Journal of the Linnean Society* **144**, 511-525 (2005).
52. K. E. Mickle, R. Lund, E. Grogan, Three new palaeoniscoid fishes from the Bear Gulch Limestone (Serpukhovian, Mississippian) of Montana (USA) and the relationships of lower actinopterygians. *Geodiversitas* **31**, 623-668 (2009).
53. L. C. Sallan, Major issues in the origin of ray-finned fish (Actinopterygii) biodiversity. *Biological Reviews* **89**, 950-971 (2014).
54. M. Friedman, The early evolution of ray-finned fishes. *Palaeontology* **58**, 213-228 (2015).
55. S. Henderson, E. M. Dunne, S. Giles, The early diversification of ray-finned fishes (Actinopterygii): h. *EarthArXiv* https://doi.org/10.31223/X58D1D (2021).
56. D. W. Bapst, M. J. Hopkins, Comparing cal3 and other a posteriori time-scaling approach in a case study with the pterocephaliid trilobites. *Paleobiology* **43**, 49-67 (2017).
57. T. A. Heath, J. P. Huelsenbeck, T. Stadler, The fossilized birth-death process for coherent calibration of divergence-time estimates. *Proceedings of the National Academy of Sciences of the USA* **111**, E2957-E2966 (2014).
58. P. M. Monarrez, N. A. Heim, J. L. Payne, Mass extinctions alter exinction and origination dynamics with respect to body size. *Proceedings of the Royal Society B* **288**, 20211681 (2021).
59. J. L. Cantalapiedra, J. L. Prado, M. Hernández-Fernández, M. T. Alberdi, Decoupled ecomorphological evolution and diversification in Neogene-Quaternary horses. *Science* **355** (2017).
60. T. Simões, O. Vernygora, M. W. Caldwell, S. E. Pierce, Megaevolutionary dynamics and the timing of evolutionary innovation in reptiles. *Nature Communications* **11**, 3322 (2020).
61. N. S. Upham, J. A. Esselstyn, W. Jetz, Inferring the mammal tree: species-level sets of phylogenies for questions in ecology, evolution, and conservation. *PLoS Biology* **17**, e3000494 (2019).
62. J. Alroy, The fossil record of North American mammals: evidence for a Paleocene evolutionary radiation. *Systematic Biology* **48**, 107-118 (1999).
63. P. A. Goloboff, J. S. Farris, K. C. Nixon, TNT, a free program for phylogenetic analysis. *Cladistics* **24**, 774-786 (2008).
64. F. Ronquist *et al.*, MrBayes 3.2: efficient Bayesian phylogenetic infernece and model choice across a large model space. *Systematic Biology* **61**, 539-542 (2012).
65. R. T. Figueroa, L. C. Weinschütz, M. Friedman, The oldest Devonian circumpolar ray-finned fish? *Biology Letters* **17**, 20200766 (2021).
66. D. L. Swofford (2003) PAUP*. Phylogenetic analysis using parsimony (*and other methods). (Sinauer Associates, Sunderland, MA).
67. N. J. Matzke, A. M. Wright, Inferring node dates from tip dates in fossil Canidae: the importance of tree priors. *Biology Letters* **12** (2016).
68. R. C. Milici, C. S. Swezey, "Assessment of Appalachian basin oil and gas resources; Devonian gas shale of the Devonian Shale-Middle and Upper Paleozoic Total Petroleum System" in Coal and Petroleum Resources in the Appalachian Basin; Distribution, Geologic Framework, and Geochemical Character: U.S. Geological Survey Professional Papper 1708*,* L. F. Ruppert, R. T. Ryder, Eds. (2014), pp. 81.
69. B. G. Gardiner, Certain palaeoniscoid fishes and the evolution of the actinopterygian snout. *Bulletin of the British Museum (Natural History) Geology* **8**, 255-325 (1963).

Figures and Tables

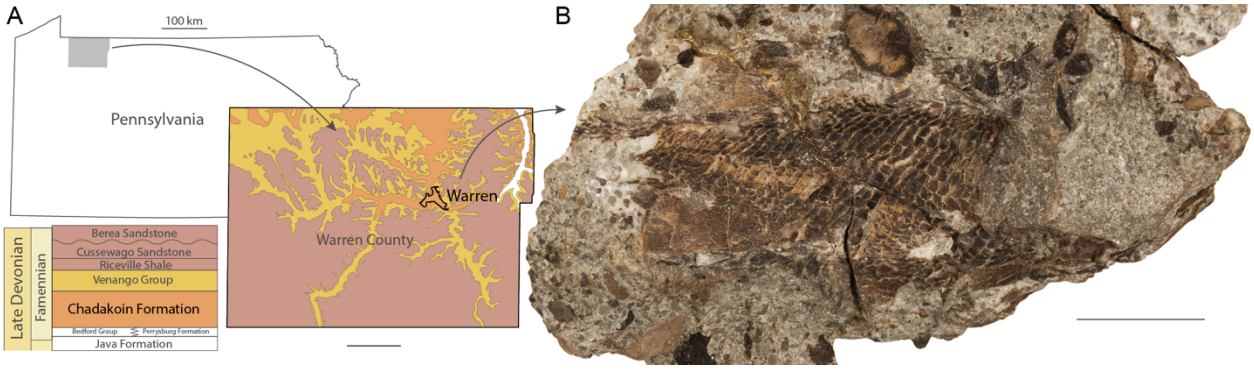

Figure 1. Geological context of MCZ VPF 5114 [new taxon name redacted from preprint]. (A) Map of Pennsylvania showing location; inset shows geological map for the area of Warren County (based on (36)) and simplified geological column (based on (68)). City of Warren indicated by solid bounding lines. (B) External photograph of MCZ VPF 5114 [new taxon name redacted from preprint] showing right lateral flank. Colors in stratigraphic column relate to geological map: latest Devonian and post-Devonian strata condensed into one color. Scale bar in (A): 10 km, in (B): 10 mm. Images copyright President and Fellows of Harvard College.

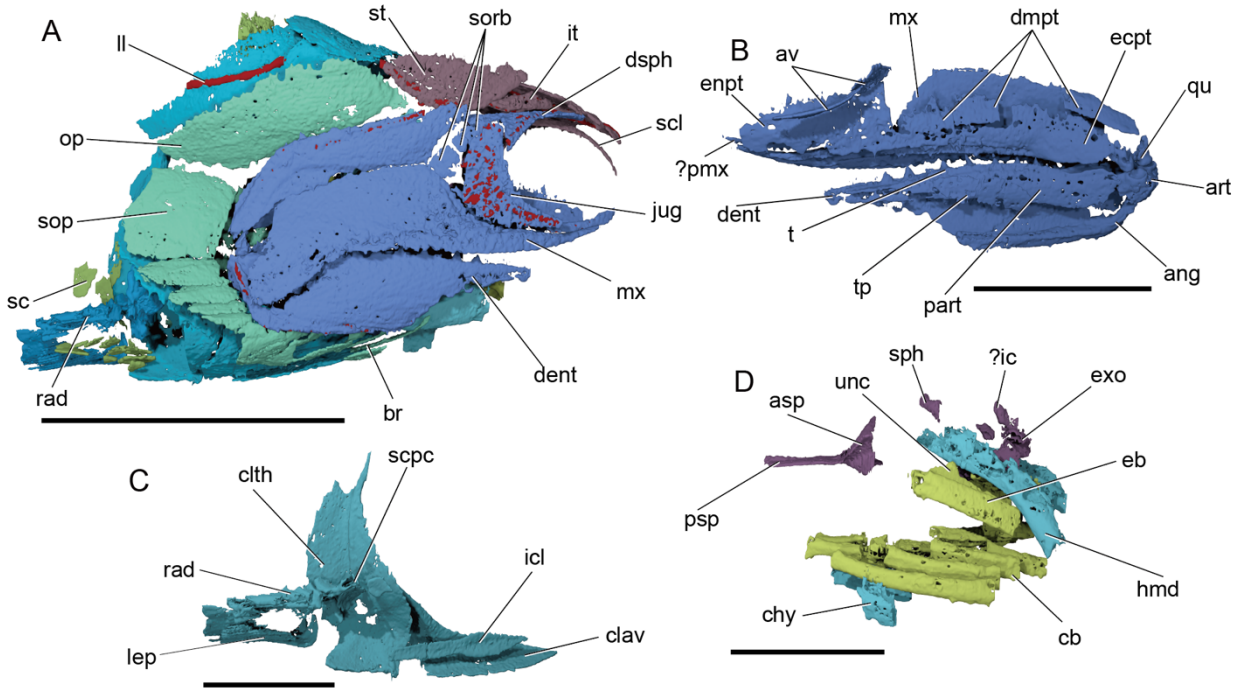

Figure 2. Anatomy of MCZ VPF 5114 [new taxon name redacted from preprint]. Renders of (A) right lateral view of specimen; (B) medial view of right upper and lower jaws; (C) medial view of left shoulder girdle and pectoral fin, and (D) left lateral view of gill skeleton, hyoid arch and braincase. Colour coding of skeleton: blue, cheek and jaw; purple, skull roof and sclerotic ossicle; pink, braincase; dark green, hyomandibula; light green, operculogular system; turquoise, shoulder girdle; yellow, gill skeleton. Scale bar in (A): 10 mm, in (B)-(D): 5 mm. Abbreviations: ang, angular; art, articular; asp, ascending process of parasphenoid; av, accessory vomer; br, branchiostegal; cb, ceratobranchial; chy, ceratohyal; clav, clavicle; dent, dentary; dmpt, dermatopterygoid; dsph, dermosphenotic; eb, epibranchial; ecpt, ectopterygoid; enpt, entopterygoid; exo, exoccipital; hmd, hyomandibula; ?ic, possible intercalar; icl, interclavicle; it, intertemporal; jug, jugal; lep, lepidotrichia; ll, lateral line; mx, maxilla; op, operculum; part, prearticular and coronoid; ?pmx, possible premaxilla; psp, parasphenoid; qu, quadrate; rad, radials; sc, scale; scl, sclerotic ossicle; scpc, scapulocoracoid; sop, suboperculum; sorb, suborbitals; sph, sphenotic ossification; st, supratemporal; t, teeth; tp, toothplate; unc, uncinate process.

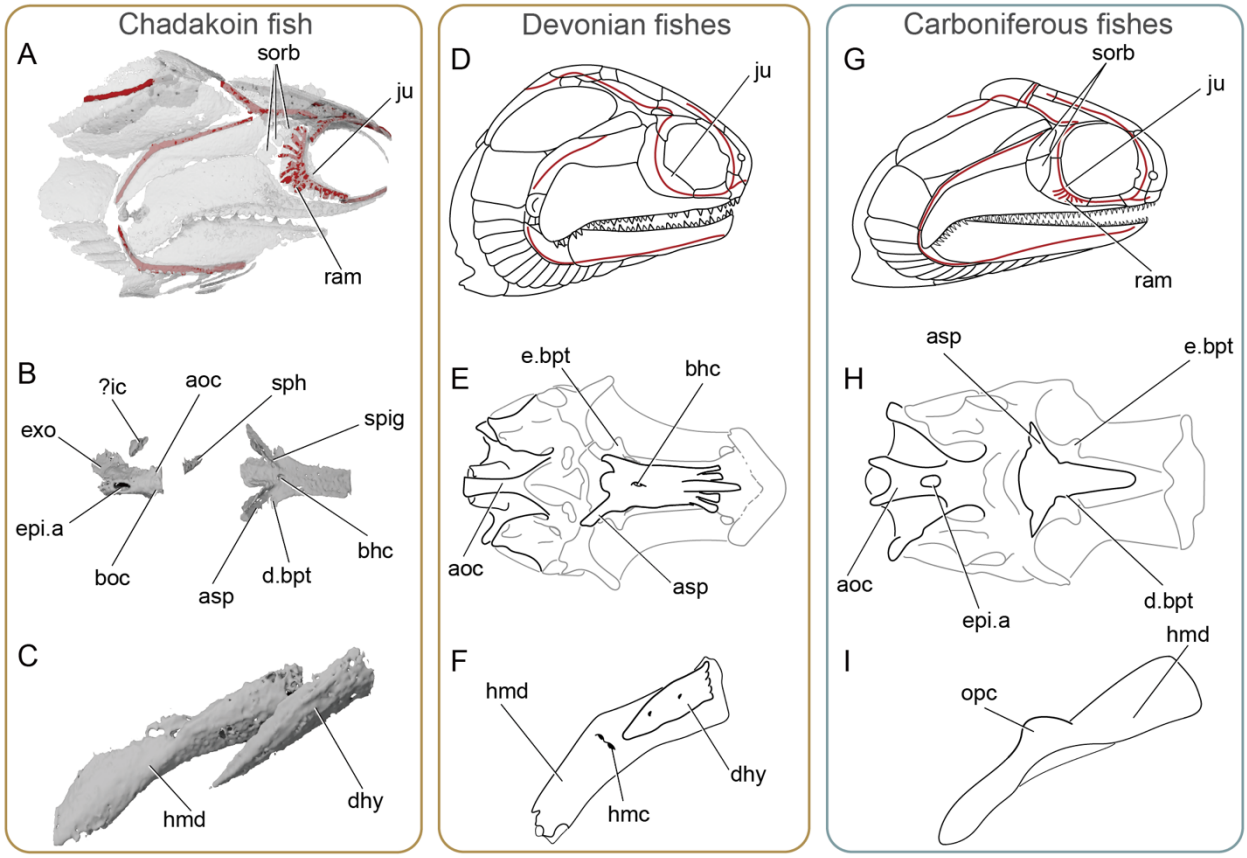

Figure 3. Comparative anatomy of MCZ VPF 5114 [new taxon name redacted from preprint] with Devonian and Carboniferous actinopterygians. Renders of MCZ VPF 5114 [new taxon name redacted from preprint] showing (A) right cheek in lateral view with sensory canals visible, (B) braincase in ventral view, and (C) right hyomandibula in lateral view. Interpretive drawings of *Mimipiscis* showing (D) right cheek in lateral view with sensory canals visible and (E) braincase in ventral view. Interpretive drawing of (F) *Moythomasia durgaringa* showing right hyomandibula in lateral view. Interpretive drawings of (G) *Cosmoptychius striatus* showing right cheek in lateral view with sensory canals visible, (H) *Lawrenciella schaefferi* showing braincase in ventral view, and (I) an indeterminate Kasimovian actinopterygian showing right hyomandibula in lateral view. Parts of the braincase are masked out in *Mimipiscis* and *Lawrenciella* to facilitate comparison with of MCZ VPF 5114 [new taxon name redacted from preprint]. (D)-(F) redrawn from Gardiner (20), (H) redrawn from Gardiner (69), (I) redrawn from Hamel and Poplin (43), and (J) redrawn from Poplin (22). Not to scale. Abbreviations: aoc, aortic canal; asp, ascending process of parasphenoid; bhc, buccohypophysial canal; boc, basioccipital; d.bpt, dermal basipterygoid process; dhy, dermohyal; e.bpt, endoskeletal basipterygoid process; epi.a, epibranchial artery; exo, exoccipital; hmc, hyomandibular canal; hmd, hyomandibula; ?ic, possible intercalar; ju, jugal; opc, opercular process; ram, ramifying tubules of infraorbital sensory canal; sorb, suborbitals; sph, sphenotic ossification; spig, spiracular groove;

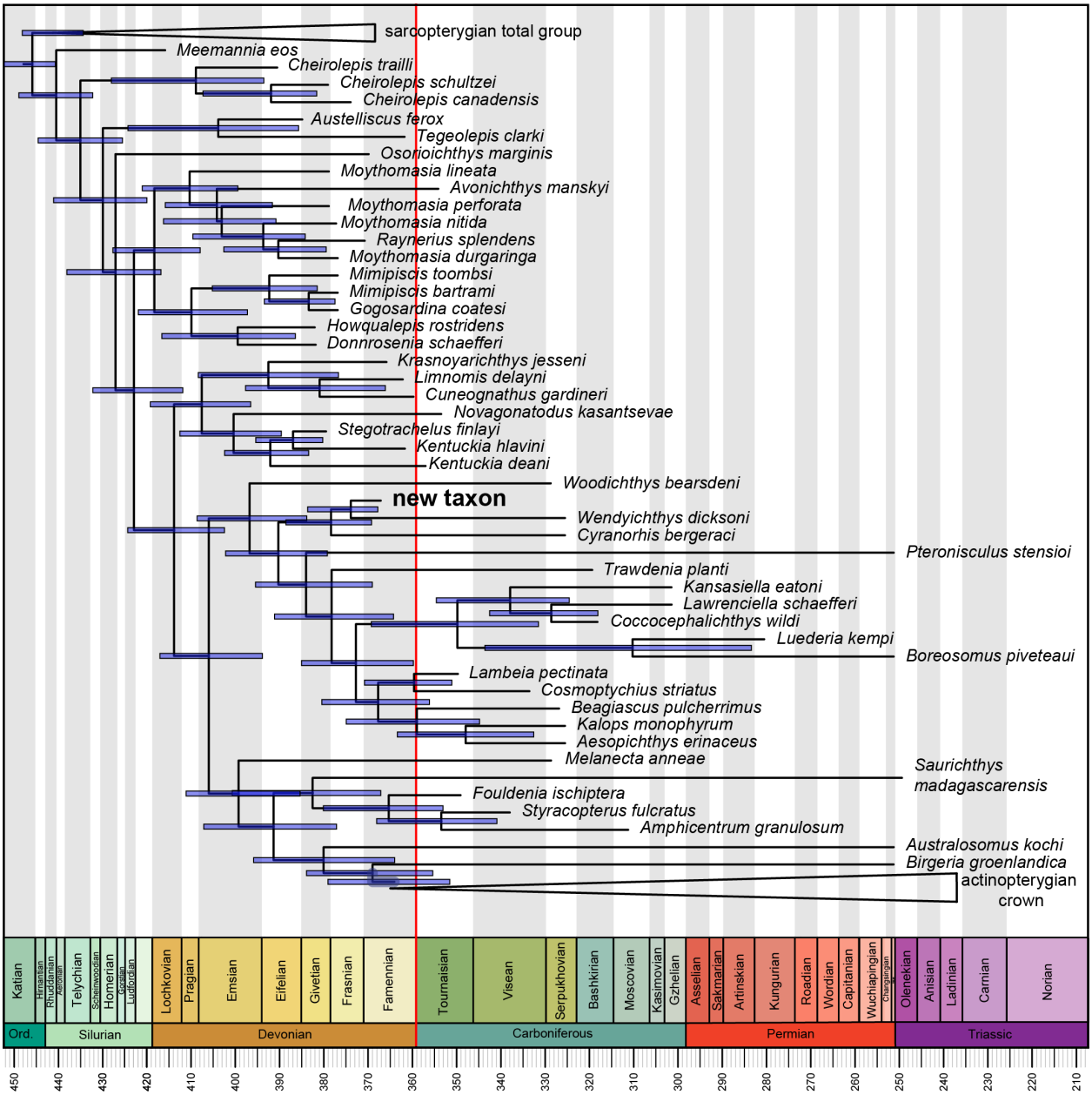

Figure 4. Timescaled phylogenetic tree. (A) Fossil birth-death analysis showing the impact of the inclusion of MCZ VPF 5114 [new taxon name redacted from preprint] and other Famennian/Tournaisian taxa on lineage survivorship over the end-Devonian Mass Extinction. Some clades collapsed for clarity; blue bars associated with nodes indicate 95% highest posterior density for age estimates. Full tree given in Fig. S8. Position of end-Devonian Mass Extinction marked by red vertical line.

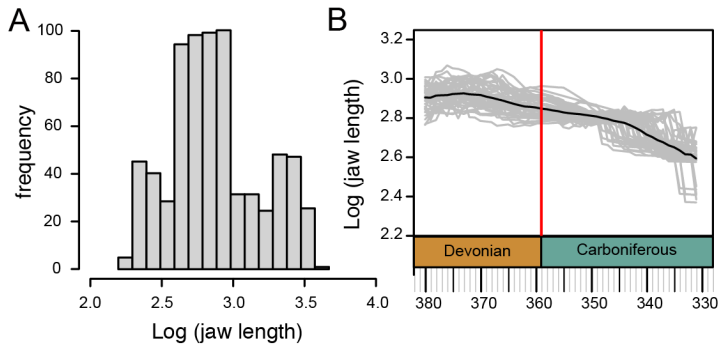

Figure 5. Patterns in early ray-finned fish size around the Devonian-Carboniferous boundary. Size represented by log-transformed lower jaw lengths. (A) Size distribution of boundary-crossing lineages estimated from a sample of 50 trees drawn from the posterior distribution of a Bayesian phylogenetic analysis using the fossilized birth-death prior. Position of end-Devonian Mass Extinction marked by red vertical line (B) Median size estimated at 1 Myr intervals (values inferred along branches plus any coincident tips) during the Late Devonian and early-mid Carboniferous. Black line indicates mean of 50 trajectories (individual grey lines) based on 50 trees drawn from the posterior sample.